RSC Advances

PAPER

View Article Online
View Journal | View Issue

Cite this: *RSC Adv.*, 2014, **4**, 25486

Thermal-healable and shape memory metallosupramolecular poly(*n*-butyl acrylate-*co*-methyl methacrylate) materials†

Zhenhua Wang, Wenru Fan, Rui Tong, Xili Lu and Hesheng Xia*

Received 31st March 2014
Accepted 28th May 2014

DOI: 10.1039/c4ra02843k

www.rsc.org/advances

A big challenge in developing stimuli-responsive materials is to integrate multiple functionalities such as shape memory property, healable ability, recyclability into a single-component material. With this purpose, we designed a novel poly(*n*-butyl acrylate-*co*-methyl methacrylate) bearing a side group 2,6-bis(1′-methylbenzimidazolyl)pyridine ligand, which is dynamically crosslinked by the metal salt zinc trifluoromethanesulfonate to obtain the metallosupramolecular polymer. The shape recovery and healing is achieved upon application of a thermal or light stimulus due to the specific metal–ligand interactions which not only serve as an "inert" crosslink network at low temperature to produce the shape recovery, but also dissociate at high temperature for healing. The healing rate is quick and the healing efficiently is close to ~90%.

Introduction

A big challenge in the development of stimuli-responsive materials is to integrate multiple functionalities such as healing ability, shape memory property and recyclability into a single-component material with good mechanical properties. Healable materials have attracted increasingly attention due to the enormous potential in the substitution for the artificial materials that always fail after micro-cracks or macroscopic damage. Those materials can be broadly classified into two categories: capsule-based healing systems and intrinsic healing systems. In the last decade, the intrinsic healable polymers based on dynamic covalent bonds[1–3] and non-covalent reversible interactions such as hydrogen bonding,[4] host–guest interaction[5] or π–π stacking[6] are of great interest owing to its dynamic nature which could be utilized to heal for multiple times. Among the non-covalent dynamic bonds, metal–ligand interactions, though owns its specific properties in various applications,[7–12] have been seldom utilized in developing healable supramolecular materials, particularly for solid materials. Rowan *et al.* reported the microphase-separated metallosupramolecular plastic that has the crack healing function by absorbing ultraviolet light to induce the dissociation of metal–ligand bond.[13] Harrington *et al.* developed a pH-responsive metal–ligand crosslinked polymer hydrogel.[14] Weng *et al.* developed healable metallosupramolecular gels based on polymers bearing 2,6-bis(1,2,3-trizaol-4-yl)pyridine ligand as side group for crosslinking.[15] Recently, Schubert *et al.* reported thermally self-healing coatings based on Fe–terpyridine binding.[16] The self-healing property was attributed to the formation of ion clusters. Nie also developed a healable gel based on the complexation of poly(acrylic acid) and Fe^{3+}.[17]

Encouraging progress in self-healing materials has been witnessed in the last decade, in some situations, however, damage in polymers often occurs in company with macroscopic deformation. Generally, the crack surfaces cannot autonomously come together to close proximity for healing without manual intervention. In some practical applications, the damaged and deformed parts cannot even be taken out for repairing. On the other hand, the lack of self-repair property in shape memory polymers always leads to limited service life, energy wasting and environmental issues. To meet this challenge, the shape memory function is introduced to the healable polymers. Shape memory alloy wires were embedded into self-healing polymers to improve the healing efficiency.[18] Mather *et al.* studied an interpenetrating network composed of crosslinked PCL, which functioned as the fixed phase for shape memory, and linear semi-crystalline PCL, which acted as the healing agent for self-healing.[19] Recently, a shape-memory assisted self-healing coating based on semi-crystalline PCL and epoxy was reported.[20] A thermally healable and shape memory polyurethane containing Diels–Alder bonds was developed by Wang.[21] Rowan and colleagues developed a light-triggered self-healing and shape memory polymer containing disulfide bonds.[22] Zhao investigated a light-triggered shape memory and healable polymer based on crosslinked crystallizing polymer and gold nanoparticles.[23] Up to now, most of the materials possessing shape-memory assisted healable property are multi-component materials. The metal–ligand crosslinked polymer

State Key Laboratory of Polymer Materials Engineering, Polymer Research Institute, Sichuan University, Chengdu 610065, China. E-mail: xiahs@scu.edu.cn

† Electronic Supplementary Information (ESI) available. See DOI: 10.1039/c4ra02843k

with both shape memory and healable properties has not been reported.

Also, polymer materials with triple shape memory functionality might enable complex, active deformations on demand, which have potential applications in intelligent medical devices, textile and assembling systems.[24] Though the great progress in shape memory polymers has been made,[25,26] the triple shape memory polymers based on metal–ligand interactions have not been reported up to now.

Herein, aiming at a single-component metallosupramolecular polymer which possesses the shape memory, healable and triple shape memory multifunctions, we introduce the dynamic metal–ligand crosslinks into molecular structure of the intrinsic shape memory polymer. As an example to illustrate this concept, the shape memory poly(butyl acrylate-*co*-methyl methacrylate) (poly(BA-MMA)) was selected because it has widely applications such as biomedical stents, coatings, *etc.*[27] The 2,6-bis(1′-methylbenzimidazolyl)pyridine (Mebip) ligand was used because of its capability of complexation with various metal ions and the reactivity of hydroxyl Mebip with the acrylic monomer, as well as thermal and light stimuli responsiveness.[13a] Recently, the effect of different metal salts on the morphology and mechanical properties of metallosupramolecular poly(*n*-butyl acrylates) was systematically studied by Jackson and coworkers.[28] However, no results on the healing properties of this material were reported. Our system has the following advantages: (1) the material reaches high healing efficiency (~90%) after only 4 min light irradiation or 25 min thermal treatment. Also, shape memory and healing can be achieved based on such materials due to following features: (i) the dynamic characteristic of metal–ligand bond, *i.e.* dissociation at higher temperature and re-formation at lower temperature, can endow the materials the self-healing function. (ii) the dynamic crosslinked network can serve as the fixed phase at lower temperature to produce the shape recovery, which is different from the blending system developed by Rowan *et al.*, in which the dynamic metal–ligand bond serves as the reversible phase for shape memory, while the covalent crosslinked network was used as the fixed phase.[12] (2) The incompatibility of metal–ligand cluster and polymer chain could produce a microphase-separated structure consisting of dispersed hard-domain nanospheres and continuous soft polyacrylates matrix, which enables the triple shape memory. (3) The controllable mechanical properties and healing efficiency can be realized by varying the monomer ratio or the metal salts type.

Results and discussion

The synthesis of the copolymer poly(BA-MMA-Mebip) is illustrated in Scheme 1. The detailed procedures are described in the ESI.† The corresponding copolymer is denoted as CP-3, CP-5 and CP-7 according to the feeding content of the ligand. The mole percentage of Mebip in the final copolymer chain is ~3.2%, ~5.3%, and ~7.6% respectively as calculated from proton NMR spectra (Fig. S8 and Table S1†) and the sequence distribution of BA and MMA monomer was tried to analysize from the ^{13}C NMR spectra (Fig. S9 and Table S2†). The GPC trace shows one broad peak for each CP series copolymer, indicating just one kind of

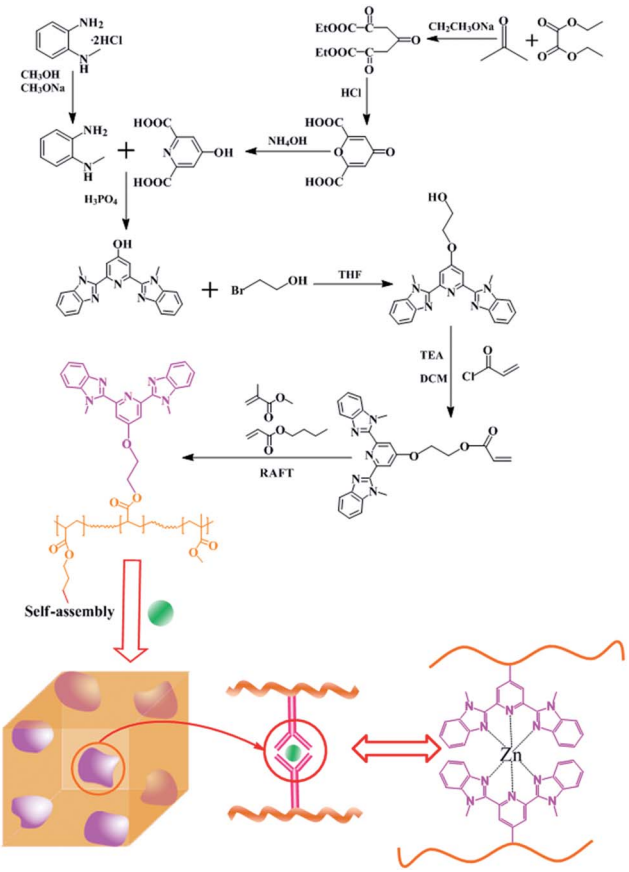

Scheme 1 Preparation of metallosupramolecular poly(BA-MMA) copolymer containing Zn–Mebip bonds.

copolymer was mainly produced (Fig. S10†). And the determined molar mass (M_n) of the copolymer CP-3, CP-5, and CP-7 from GPC is 13515, 9815, and 9781 g mol^{-1} respectively (Table S4†). The poly(BA-MMA-Mebip) copolymers are further crosslinked by adding metal salt zinc trifluoromethanesulfonate ($Zn(OTf)_2$) to obtain the crosslinked metallosupramolecular poly(BA-MMA). The crosslinking by $Zn(OTf)_2$ leads to the formation of a gel *via* metal–ligand interactions. As a control experiment, we also used the europium trifluoromethanesulfonate ($Eu(OTf)_3$) as a crosslinking agent. After adding the $Eu(OTf)_3$, the Eu-based copolymer mixture turns highly viscous rather than a gel state like Zn-based system, indicating the weaker binding of Eu–Mebip compared with Zn–Mebip. To prepare the solid MSP, the solvent in the gel was removed in vacuum. The obtained solid polymer was further compression molded into a rectangle sheet of 1 mm thickness. The corresponding crosslinked MSP materials with a Mebip mole percentage of 3.2%, 5.3% and 7.6% were designated as MSP-3, MSP-5 and MSP-7 respectively. The prepared control sample Eu–Mebip bonded poly(BA-MMA) materials was designated as "Control-1". For comparison, and the normal ethyleneglycol dimethacrylate (EGDMA) chemically crosslinked poly(BA-MMA) material was also prepared and designated as "Control-2". The linear poly(BA-MMA) was designated as "Control-3" which is a flowing liquid at 25 °C and cannot be processed into solid material.

Rheological properties of metallosupramolecular gels

To investigate the role of Zn–Mebip crosslinks within the polymer, rheometer tests were conducted. The dried metal–ligand crosslinked polymer (MSP-5) was re-swelled for 24 h in 1,1,2,2-tetrachloroethane to form a transparent gel. Fig. 1a shows the storage modulus G' and loss modulus G'' or MSP series samples with the time. The storage modulus (G') of MSP-3, MSP-5, and MSP-7 reaches ~230 Pa, ~2300 Pa and ~5500 Pa respectively. The metal–ligand interaction plays a vital role in the construction of the supramolecular dynamic cross-linking network. Higher Mebip content results in a stronger storage modulus due to a higher crosslinking density. To illustrate the reversibility of the Zn–Mebip interactions, we conducted the sol–gel experiments. As shown in Fig. 1b, after treatment at 140 °C (corresponding to the flow temperature of MSP-5 as disclosed below) for 10 min, the formed gel turns into a viscous and flowable sol due to the collapse of the supramolecular network resulted from the cleavage of metal–ligand bonds. Upon cooling, the gel appears again, due to the rebuilding of the crosslinking network arising from the recombination of metal–ligand interactions.

Microphase separation of metallosupramolecular poly(BA-MMA) copolymer

The effect of Mebip content on the thermal behaviors of the copolymer CP series and metallosupramolecular MSPs were studied by differential scanning calorimetry (DSC) and dynamic mechanical thermal analysis (DMTA). For CP series copolymers, DSC traces (Fig. 2a) suggests that the glass transition temperature T_{g1} for CP-3, CP-5 and CP-7 is ~−0.5 °C, ~6.4 °C and ~15.2 °C respectively, showing an increase trend with the ligand

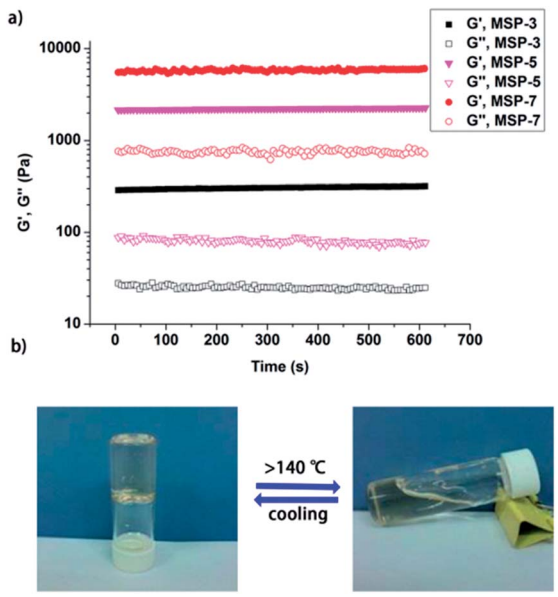

Fig. 1 (a) The storage modulus G' and loss modulus G'' as a function of time (strain = 1%, frequency is 1 Hz) for MSP swelled in 1,1,2,2-tetrachloroethane with a concentration of 100 mg ml^{-1}. (b) Thermally responsive sol–gel transition.

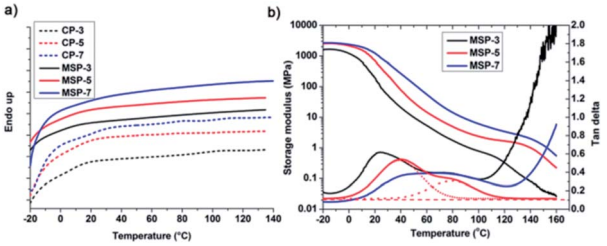

Fig. 2 (a) DSC curves of CP series and MSP series with various ligand contents. (b) DMTA traces of MSP series with various amounts of Zn–Mebip bonds, the peaks of tan δ were fitted by Gaussian function to ascertain the T_{g2}.

content. The T_{g1} signals for solid MSPs in DSC traces become weaker as increasing the metal–ligand content. The possible reason is that the crosslinked network will restrict the segment movement to some degree. For solid MSP series, DMTA curves (Fig. 2b) reveal two different phase transition temperatures, together with the viscous flow temperature. The first one is glass transition temperature of free soft polyacrylate chains (T_{g1}), and the second one is defined as T_{g2}, possibly associated with the glass transition temperature of the molecular chains in the metal–ligand rich hard domains resulted from microphase separation, and the third one is the flow temperature (T_f) which is associated with the breakage of dynamic metal–ligand network and polymer liquefying. The three temperatures are key factors for shape memory and healing and triple shape memory. The T_{g1} determined by DMTA for MSP-3, MSP-5 and MSP-7 are ~24.0 °C, ~39.0 °C and ~46.8 °C, respectively (Fig. 2b). The T_{g2} was determined by a Gaussian fitting for the tan(δ) peak as shown in Fig. 2b. The T_{g2} for MSP-3, MSP-5 and MSP-7 is ~68.4 °C, ~79.1 °C for and ~83.0 °C respectively. The T_f can provide the estimation for the dissociation temperature of the metal–ligand bond. When the temperature is higher than T_f, the materials start to flow, leading to a rapid decrease in the storage modulus. The T_f for MSP-3, MSP-5 and MSP-7 are ~95 °C, ~140 °C and ~160 °C respectively. All the transition temperature shows an increasing trend with increasing the metal ligand content. For the controlled Eu-based MSP sample, the T_{g2} is not observed in the tan δ curves of DMTA because of the absence of microphase separation in Eu-based material (Fig. S11†).

A few researchers suggested that micro-phase separation in Mebip-based metallosupramolecular polymer system can produce hard micro-domains.[13,28,29] In order to confirm the occurrence of micro-phase separation; we conducted transmission electron microscopy (TEM), wide angle X-ray diffraction (WAXD), and small-angle X-ray scattering (SAXS) characterization. TEM indeed reveals a clear two-phase morphology for sample MSP-5, with nanospheres of an average size ~60 nm dispersed in a continuous poly(BA-MMA) matrix (Fig. 3a). The size distribution of nanospheres is shown in Fig. 3b. This structure is not reported in the former metallosupramolecular polyacrylates system[16,28] and it is different with lamellar structure revealed in the main chain metallosupramolecular polymers.[13a] The nanospheres are formed by microphase separation, *i.e.* the further aggregation of Zn–Mebip

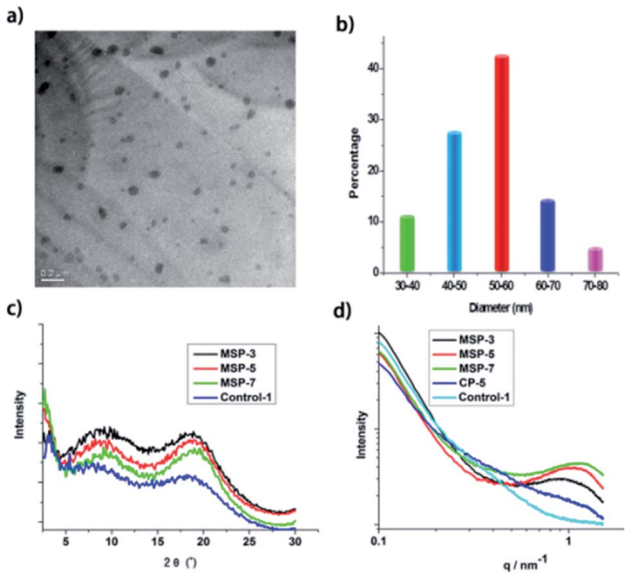

Fig. 3 (a) TEM image of MSP-5 sample. (b) Size distribution of hard domain in MSP-5 sample. (c) WAXD patterns of MSPs with various Mebip contents. (d) SAXS patterns of MSP series, CP-5 and Control-1.

clusters. The microphase separation is responsible for the extra glass transition temperature of molecular chains around the metal–ligand rich hard domains and also it is believed that the microphase separation contributes to an improvement in the mechanical properties of the materials.

Fig. 3c shows that two peaks are presented in the WAXD patterns: the peak $2\theta \sim 20^\circ$ corresponds to the amorphous halo; another peak at $d = 10.4$ Å ($2\theta \sim 8.5^\circ$) is assigned to the metal-to-metal distance within the hard phase on the basis of previous research.[28,29] In contrast to MSP-5, the peak of Control-1 sample at $d \sim 10.4$ Å is weak, indicating a decreased packing of metal–ligand in the Eu-based material. SAXS was used to confirm the formation of Zn–Mebip cluster. The scattering patterns for all MSP series samples (Fig. 3d) reveal a broad scattering peak. The long period calculated from SAXS curve deceases from 7 nm to 5.2 nm as metal–ligand complexes content increases from 3.2% (MSP-3) to 7.5% (MSP-7). For the scattering patterns of both Eu-based sample (Control-1) and copolymer sample (CP-5), no scattering peaks are observed in the SAXS curves. These results suggest that the Zn ion plays an important role to the formation of metal–ligand clusters.

Mechanical and healing properties

The copolymer poly(BA-MMA-Mebip) is an amorphous tacky solid with very weak mechanical properties. After crosslinking with metal salt, the MSP series samples have good and adjustable mechanical properties. The mechanical properties of MSP materials and the control samples are summarized in Table 1. With increasing the metal–ligand amount, the tensile strength and Young's modulus increase, while strain at break decreases. MSP-3 is most extensible and MSP-7 is the stiffest, while MSP-5 seems to have a good balance between the strength and elongation. The type of metal salt has a strong effect on the

Table 1 Mechanical and self-healing properties of MSP[a]

Sample	Young's modulus (MPa)	Tensile strength (MPa)	Strain at break (%)	Healing efficiency*
MSP-3	3.6 ± 0.2	4.4 ± 0.2	242 ± 12	98 ± 12
MSP-5	34.6 ± 2.5	9.7 ± 0.6	144 ± 23	88 ± 18
MSP-7	143 ± 10.6	12.5 ± 1.5	63 ± 25	65 ± 32
Control-1	18.1 ± 1.9	8.3 ± 0.6	507 ± 51	7 ± 3
Control-2	232.3	9.2	50	0

[a] * healing efficiency is calculated based on the recovery in the elongation at break. Strain rate: 50 mm min^{-1}. Control-1 is Eu-based MSP material. Control-2 is chemically crosslinked poly(BA-MMA-EGDMA).

mechanical properties of metallosupramolecular material. Compared with Zn-based material (MSP-5), the Eu-based material (Control-1) exhibits lower tensile strength but a better elasticity due to the weaker binding of Eu–Mebip bond. The tensile strength and strain at break of MSP-5 are both almost two-fold of the reported optically healable main-chain metallosupramolecular material assembled from poly(ethylene-*co*-butylene) functionalized with Mebip.[13a] On the other hand, for the chemical crosslinked sample (Control-2), the strain at break decreases by ~66% compared with that of MSP-5 while the tensile strength shows almost no difference. The linear poly(BA-MMA) without any crosslinking prepared in this study is viscous at room temperature and could not be molded into solid material. Therefore, it is convinced that the unique mechanical properties of the Zn-based MSP materials are related to the formation of microphase-separated structure composed of hard Zn–Mebip hard micro-domains and soft polyacrylate phases.

For previous healable metallosupramolecular materials,[13–17] the crack interface cannot autonomously contact together once damaged with considerable strain at break. Therefore the ability to automatically bring the separated damaged area together under external stimulus is of great significance. Our prepared MSPs have the ability to realize shape memory and healing under thermal or light stimulus due to its special structure as stated above. To testify this, we firstly cut the MSP specimen by ~70% depth of sample thickness, and then kept the crack surfaces separated at a bending angle of ~90° for 10 min at room temperature. After removing the stress, a crack with large deformation was produced. The shape memory and healing was realized by simply heating the sample to 140 °C for a certain time to induce the consequent occurrence of shape recovery, crack surfaces closure and crack healing. Fig. 4d shows the pictures of the shape memory and healing process, and Fig. 4a and b are digital microscopy with a depth-of-field. The proposed mechanism is illustrated in Fig. 4c. For the MSP materials suffered damage with large deformation, as the sample temperature was heated above T_{g1}, the separated crack surfaces start to approach each other. Further heating the sample will speed up the shape recovery to close the crack surfaces. When the sample temperature reaches the temperature which is sufficient to induce the dissociation of metal–ligand bonds, network de-crosslinking, material liquefying, and consequent

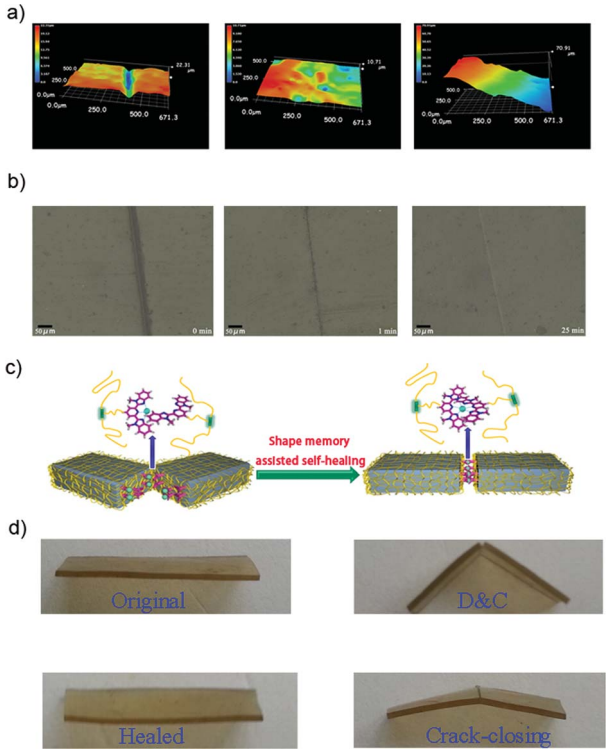

Fig. 4 (a) 3D optical photographs of healing process of MSP-5 *via* digital microscope with a depth-of-field. (b) Digital images for healing process of MSP-5. (c) Schematic illustration for thermal-induced shape memory assisted healing of the metallosupramolecular materials. (d) Digital pictures of shape memory assisted self-healing process of MSP-5. Deformation and cracking at room temperature, healing temperature is 140 °C, healing time 25 min.

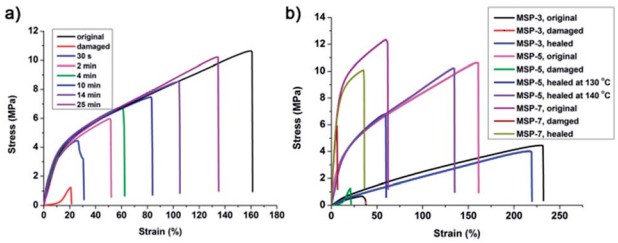

Fig. 5 Mechanical and self-healing properties for MSP series samples. (a) Stress–strain curves of damaged MSP-5 sample healed at various times, healing temperature T = 140 °C. (b) Stress–strain curves of original, damaged and healed MSP series samples, healing time is 25 min.

fast polymer chain diffusion and re-entanglement will occur. Upon cooling the material cracks will be healed and the mechanical properties will be recovered.

The healing efficiency is calculated based on the strain recovery and the data are shown in Table 1. Fig. 5a shows that the stress and strain for the damaged MSP-5 specimen recovered with the contact time. After heating for ~25 min at 140 °C, the healing efficiency of the damaged MSP-5 reaches ~88%. We noted that during tensile test some healed samples did not break at the damaged site but in other places, indicating that the healing efficiency is progressed to a considerable level. Fig. 5b shows that the healing efficiency of MSP series with different contents of metal–ligand bond at 140 °C is different. A higher amount of metal–ligand bond leads to a lower healing efficiency at 140 °C. This is attributed to the different temperature of MSP series required for the metal–ligand decomplexation and material liquefying (Fig. 2b). At 140 °C, MSP-3 is near completely liquefied and the molecular chains have the best mobility so that the dynamic metal–ligand motifs between two crack interfaces have the maximum probability to reach and recombine, resulting in a highest healing efficiency of ~98%. While for MSP-7, it is only partially liquefied at 140 °C and the chain mobility is very limited, leading to a lower healing efficiency of ~65%. It can be noted in Fig. 5b that a lower healing efficiency (~58%) for MSP-5 was obtained at a temperature of ~130 °C, which is much lower than T_f of MSP-5. At a temperature between 55 °C and 95 °C, shape recovery is good, but the healing efficiency is very low and can be negligible. For general healable metallosupramolecular materials, the healing temperature is usually high in order to achieve the dissociation of metal–ligand bonds and better mobility of polymer molecular chains, which are crucial for high healing rate and healing efficiency. For example, the temperature of optically healable polymer went up to 190 °C and 220 °C for La-based and Zn-based system respectively upon UV irradiation.[13a] In another work, the temperature required to heal the crack was above 100 °C for metal–ligand crosslinked polyacrylate and the healing time last for several days.[16] The healing temperature for metallosupramolecular materials is relatively high, comparable to the melting or softening temperature for normal linear amorphous or crystalline polymers. However the healing mechanism is different from the thermal welding. For traditional polymers, the ability to heal the damage is really poor due to the slow rates of diffusion and re-entanglement of the chains which are inversely proportional to the molecular mass.[30] For normal covalent crosslinked polymer, *e.g.* sample "Control-2" in this study, it is difficult to be self-healed even under high temperature. For MSP materials, the dynamic metal–ligand crosslinks can be broken to form the liquefied linear low-molar-mass species on exposure to heat. The molecular weight of the CP series poly(BA-MMA) copolymer which can be produced after de-crosslinking is lower (~10 000) and thus the rates of chain diffusion and re-entanglement are much faster compared to normal amorphous polymers (Mn > 100 000). This leads to a high healing efficiency for metallosupramolecular polymer materials.

All the results indicate that T_f related to the dissociation of metal–ligand bond is a key factor for healing. It must be pointed out that this result is different from the normal intrinsic healing polymer in which an increase in the content of dynamic bonds will lead to a better healing efficiency, this is because that in our system, the realization of healing is not only by the re-formation of metal–ligand bonds in the crack surface, but also by the chain diffusion and re-entanglement caused by the metal–ligand network de-crosslinking and material liquefying.

To illustrate the intrinsic nature of shape memory and healing process, we also studied the healing behavior for three

control samples. For covalent crosslinking poly(BA-MMA-EGDMA) (Control-2), almost no healing can be observed, indicating that the contribution of the molecular chain entangling to the healing property is very limited. For Eu-based MSP (Control-1), the healing efficiency is only ~7% which is much lower than that of Zn-based MSP-5. Europium as lanthanide group element shows more dynamic and weaker binding with Mebip ligand. Previous research[12] showed that the temperature (T_f) that is sufficient to disrupt the Eu–Mebip bond and make material flow is only ~40 °C. The T_g of Control-1 is ~43 °C (Fig. S10†). The T_f is too close to the T_g, which will hamper the self-healing of materials. When the sample Contro-1 is heated above its flow temperature, the Eu–Mebip interactions sufficiently dissociate. Upon cooling below 40 °C, the Eu–Mebip interactions could not efficiently be recombined because the molecular chains were frozen below the T_g. Chain mobility is a key factor for the healing process. Therefore, for MSP materials, T_f should be much higher than T_g to assure the necessary chain mobility during healing to achieve the re-formation of metal–ligand bond. Zn-based MSP material meets such a requirement while Eu based MSP does not.

To explore whether the shape memory and healing process could be triggered by light, we conducted the experiment under UV irradiation. After the sample was deformed and cracked at room temperature, it was exposed to ultraviolet radiation with a wavelength of 300–400 nm and an intensity of 127 mW cm^{-2}. An exposure of 4 min is sufficient to bring the crack surfaces together and heal the crack (Fig. 6a). *In situ* measurements revealed that the UV irradiation could give rise to a surface temperature rise of 185.1 °C (23.9 °C to ~208.0 °C) for MSP-7 in 4 min (Fig. 6b). As the Zn–Mebip content increases, the slope of the curve (which is proportional to the increasing rate in surface temperature) becomes steeper. At a lower Zn–Mebip content (MSP-3), the surface temperature rise decreased to 120.1 °C, indicating the vital role of Zn–Mebip interaction in the photothermal conversion process. This is further evidenced by the surface temperature rise ~90.4 °C (from 22.3 °C to 121.7 °C) for Control-2 sample without Zn–Mebip motif during 4 min UV irradiation. Fig. 6c shows that the healing efficiency in 4 min UV irradiation is very high, close to 100%, The reason is that UV induced the surface temperature rise can lead to the decomplexation of Zn–Mebip, consistent with result of the previous report.[13a]

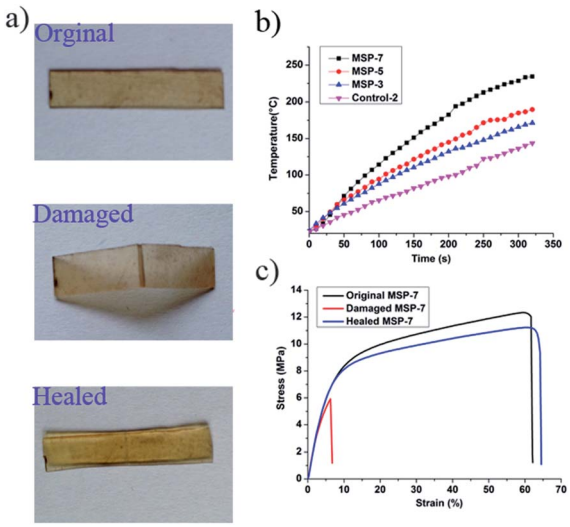

Fig. 6 Optical triggered shape memory assisted self-healing of MSP-7. (a) Optically healing of MSP-7 on exposure to ultraviolet radiation with a wavelength of 300–400 nm and an intensity of 127 mW cm^{-2}; (b) surface temperature of samples on exposure to same conditions, as a function of time, determined with an infrared camera. (c) Stress–strain curves of films of MSP-7, shown are data for original, damaged, and healed samples (width, 10.1 mm; depth, 0.56 mm).

Triple shape memory property

Triple shape memory polymer is an important smart material in the shape memory polymers.[24–26] Triple shape memory polymer can change shapes twice and can fix two metastable shapes in addition to its permanent shape. Triple shape memory has not been reported in the metallosupramolecular materials up to now. Two reversible thermal transitions of MSP series materials including two glass transition, together with metal–ligand bond crosslinked network below the flow temperature, can lead to a triple shape memory function.

The temporary shape was fixed *via* a two-step programming as follows: firstly, the rectangle sheet specimen was heated to 95 °C, a temperature higher than T_{g2}, at which the sample was in elastic state, and then it was shaped into a temporary twisted "V" shape under external stress. Then the sample was cooled to 55 °C (a temperature higher than T_{g1} but lower than T_{g2}) and maintained for 10 min under external stress, after the stress was released, twisted "V" shape was fixed with internal stress stored in the specimen. The first temporary shape fixation is attained by the T_{g2}. Secondly, the specimen was re-shaped from "V" to "S" shape under external stress at 55 °C, the sample was then cooled to 10 °C and after removing the stress, temporary shape "S" was fixed with internal stress. The second temporary shape fixation is attained by the frozen chain below the T_{g1}.

The shape recovery process is realized by heating (Fig. 7). When the sample was heated to 55 °C, the frozen chains start to move, the temporary shape "S" was changed to twisted shape "V", which can be remained at 55 °C. Further increasing the temperature to 95 °C, the twisted shape "V" was changed to the original rectangle sheet shape due to the release of internal stress. For the Eu-based MSP (Control-1), triple shape memory cannot be realized due to the lower flow temperature and the absence of microphase separation (Fig. S11†).

Fig. 7 Triple shape memory process of metallosupramolecular MSP-5.

Conclusions

In summary, we realized the healing and triple shape memory based on a single-component metal–ligand crosslinked supramolecular material. Two main structure criteria for this kind of materials are proposed: (1) the existence of two glass transitions (T_{g1} and T_{g2}) of polymer chains resulted from microphase separation; (2) the dissociation temperature of metal–ligand band (T_f) must be higher than T_{g1} and T_{g2}. As an example, the metallosupramolecular copolymer poly(BA-MMA) bearing a Mebip ligand, crosslinked by metal zinc salt was prepared and investigated. This novel material has a microphase separated two-phase structure composed of soft polyacrylate phases and metal–ligand rich hard domains, and has three reversible phase transitions, which enables the materials with shape memory, healing and triple shape memory functions. The materials have good mechanical strength and healing efficiency close to 90%, and those properties can be systematically tuned by a diversity of molecular parameters. The realization of healing is not only by the re-formation of metal–ligand bonds in the crack surface, but also by the chain diffusion and re-entanglement caused by the metal–ligand network de-crosslinking and material liquefying under external thermal or light stimulus. The concept of integrating healing and triple shape memory into a single-component material by introducing metal–ligand bond into the molecular structure of intrinsic shape memory polymer seems to be applicable to a wide range of other dynamic supramolecular polymer systems.

Materials and methods

Materials preparation

The synthetic route is shown in Scheme 1. The synthesis of 4-hydroxy-2,6-bis-(1′-methyl-benzimidazolyl)pyridine (compound 1, HO-Mebip) and 2-(2,6-bis(1-methyl-1*H*-benzo[*d*]imidazol-2-yl) pyridin-4-yloxy)-nonan-1-ol (compound 2, BIP-OH) are shown in the ESI.†

Synthesis of 2-(2,6-bis(1-methyl-1*H*-benzo[*d*]imidazol-2-yl)-pyridin-4-yloxy)nonyl acrylate (compound 3, Mebip-Ac). The self-made compound 2, *i.e.* BIP-OH (6 g, 15.0 mmol), triethylamine (3.4 ml, 24.4 mmol), dichloromethane (600 ml) were charged to a 1 l round bottom flask, then the solution was kept stirring at 0 °C for 2 h. The acryloyl chloride (2 ml, 24.5 mmol) dissolved in dichloromethane (20 ml) was added into the above solution dropwise and the mixture was left to react for 4 h at 0 °C, then 24 h at room temperature. The product was collected and was further purified *via* column chromatography (CH_2Cl_2/MeOH) using the silica as the stationary phase.

Synthesis of poly(BA-MMA) copolymer containing ligand (CP series). Butyl acrylate, methyl methacrylate, monomer compound 3 (Mebip-Ac), initiator, *S*,*S*′-bis(*R*,*R*′-dimethylacetic acid) trithiocarbonate, were charged into dry DMF solvent, then the mixture was reacted at 70 °C for 24 h under nitrogen. The polymerization recipes are listed in Table S1.† After polymerization, the solution was poured into cold MeOH–H_2O (9 : 1) mixture to obtain polymer precipitate, and then dried in vacuum at 50 °C.

Synthesis of the metallosupramolecular copolymer. Typically, in a 50 ml beaker the desired amount of the self-made copolymer (CP series) was dissolved in chloroform (100 mg ml^{-1}). The $Zn(OTf)_2$ or $Eu(OTf)_3$ in acetonitrile (100 mg ml^{-1}) was added into the copolymer solution. The amount of metal salt added was adjusted to provide for metal : ligand equivalents of 1 : 2 or 1 : 3 (accounting for 1 : 2 and 1 : 3 binding, respectively). The mixture turned into gel in 1 min after adding $Zn(OTf)_2$. On addition of $Eu(OTf)_3$, the system turned into a viscous fluid rather than a gel. The mixtures were then dried at 70 °C for 4 h and overnight at 80 °C to remove the solvent in vacuum. The as-prepared solids were compression moulded at 170 °C for Zn-based system and 130 °C for Eu-based system to obtain semi-transparent yellow rectangle sheets with a thickness of ~1 mm (accounting for different bond strength of Zn–Mebip and Eu–Mebip).

Shape memory and thermal healing test

Thermally induced shape memory and self-healing experiment was conducted as follows: the MSP specimen was cut by ~70% depth of sample thickness. The crack depth was determined *via* a razor with length scale calibrated by a caliper. The crack surfaces were then kept separating at a bending angle of ~90° for 10 min at room temperature. After removing the stress, a crack with large deformation was produced. The shape memory and self-healing was realized by simply heating the sample to 140 °C in an oven for a certain time.

Light triggered shape memory and self-healing experiment was conducted as follows: the sample was cracked and deformed as the procedures described above, then was exposed to a filtered light source with wavelengths 300–400 nm at an intensity of 127 mW cm^{-2} for 4 min. The surface temperature rise was *in situ* measured by an infrared camera.

General methods

The NMR spectra were recorded at room temperature on a 400 MHz Brucker Avance II 400 spectrometer. Chemical shift were referenced to the solvent values (for DMSO-d_6, $\delta = 2.49$; for $CDCl_3$, $\delta = 7.25$). Molecular weight was measured with gel permeation chromatography (GPC, TOSOH, HLC-8320GPC) with THF as the eluent at a flow rate of 0.6 ml min^{-1} at 40 °C. Molecular weight was calibrated with polystyrene standard. The photo-luminesence emission spectra were recorded at FL-4000 (excitation wavelength = 300 nm). Rheological measurements were measured using parallel plate geometry. The plate used has a diameter of 25 mm and the gap is set at 1 mm for all measurements. The measurement of mechanical properties was conducted on a universal testing machine (Instron 5567, US) at room temperature with a strain rate 50 mm min^{-1}. DSC curves were measured on a Q20 instrument (TA instruments, USA). The samples were annealed at 160 °C for 5 min during the first heating ramp. After cooling to −30 °C at a cooling rate of 10 °C min^{-1}, the T_g was measured on the second heating ramp in the temperature range of −30–150 °C at a heating rate of 10 °C min^{-1}. The dynamical mechanical tests were performed on a Q-800 instrument (TA Instruments, USA) with tensile mode. The

storage modulus (G') and loss factor (tan δ) were measured in the temperature range of −20–160 °C at a heating rate of 3 °C min^{-1}. The dimension of the rectangle sample strips was 35 × 10 × 1 mm^3. Observation of digital microscope with a depth-of-field resolution was performed at VHX-1000C (KEYENCE, Japan). WAXD tests were conducted on a BRUKER D8 discovery rotating anode diffractometer using Cu Ka radiation of wavelength 0.1542 nm with a VANTEC-1 detector. The goniometer scanned diffracted X-rays in the range $2\theta = 2$ to 30°. SAXS experiments were performed on a NanoSTAR-U (BRUKER AXS INC.) with Cu Kα radiation of wavelength 0.154 nm. The generator was operated at 40 kV and 650 μA. Two-dimensional SAXS patterns were obtained using a HI-STAR detector. The sample to detector distances were LSD = 1074 mm. The effective scattering vector q ($q = 4\pi \sin \theta/\lambda$, where 2θ is the scattering angle) at this distance ranges from 0.044 to 2.0 nm^{-1}. TEM was performed using a FEI Tecnai G^2F20 S-TWIN transmission electron microscope, operating at an accelerating voltage of 200 kV.

Acknowledgements

H.S. Xia acknowledges financial support from the major project of Chinese Ministry of Education (313036) and the Programme of Introducing Talents of Discipline to Universities (B13040), and National Natural Science Foundation of China (51203102).

Notes and references

1 (*a*) X. Chen, M. A. Dam, A. Ono, A. Mal, H. Shen, S. R. Nutt, K. Sheran and F. Wudl, *Science*, 2002, **295**, 1698; (*b*) X. Chen, F. Wudl, A. K. Mal, H. Shen and S. R. Nutt, *Macromolecules*, 2003, **36**, 1802.

2 (*a*) Y. Amamoto, J. Kamada, H. Otsuka, A. Takahara and K. Matyjaszewski, *Adv. Mater.*, 2011, **50**, 1660; (*b*) Y. Amamoto, H. Otsuka, A. Takahara and K. Matyjaszewski, *Adv. Mater.*, 2012, **24**, 3975.

3 G. Deng, C. Tang, F. Li, H. Jiang and Y. Chen, *Macromolecules*, 2010, **43**, 1191.

4 (*a*) P. Cordier, F. Tournilhac, C. Soulie-Ziakovic and L. Leibler, *Nature*, 2008, **451**, 977; (*b*) Y. Chen, A. M. Kushner, G. A. Williams and Z. Guan, *Nat. Chem.*, 2012, **4**, 467; (*c*) J. Hentschel, A. M. Kushner, J. Ziller and Z. Guan, *Angew. Chem., Int. Ed.*, 2012, **51**, 10561.

5 (*a*) M. Zhang, D. Xu, X. Yan, J. Chen, S. Dong, B. Zheng and F. Huang, *Angew. Chem., Int. Ed.*, 2012, **51**, 7011; (*b*) M. Nakahata, Y. Takashima, H. Yamaguchi and A. Harada, *Nat. Commun.*, 2011, **2**, 511.

6 S. Burattini, H. M. Colquhoun, J. D. Fox, D. Friedmann, B. W. Greenland, P. J. F. Harris, W. Hayes, M. E. Mackay and S. J. Rowan, *J. Am. Chem. Soc.*, 2010, **132**, 12051.

7 G. R. Whittell, M. D. Hager, U. S. Schubert and I. Manners, *Nat. Mater.*, 2011, **10**, 176.

8 S. J. Payne, G. L. Fiore, C. L. Fraser and J. N. Demas, *Anal. Chem.*, 2010, **82**, 917.

9 K. L. Robinson and N. S. Lawrence, *Anal. Chem.*, 2006, **78**, 2450.

10 A. Piermattei, S. Karthikeyanm and R. P. Sijbesma, *Nat. Chem.*, 2009, **1**, 133.

11 R. T. M. Jakobs and R. P. Sijbesma, *Organometallics*, 2012, **31**, 2476.

12 J. R. Kumpfer and S. J. Rowan, *J. Am. Chem. Soc.*, 2011, **133**, 12866.

13 (*a*) M. Burnworth, L. Tang, J. R. Kumpfer, A. J. Duncan, F. L. Beyer, G. L. Fiore, S. J. Rowan and C. Weder, *Nature*, 2011, **472**, 334; (*b*) S. Coulibaly, A. Roulin, S. Balog, M. V. Biyani, E. J. Foster, S. J. Rowan, G. L. Fiore and C. Weder, *Macromolecules*, 2013, **47**, 152.

14 N. Holten-Andersen, M. Harrington, H. Birkedal, B. P. Lee, P. B. Messersmith, K. Y. C. P. Lee and J. H. Waite, *Proc. Natl. Acad. Sci. U. S. A.*, 2011, **108**, 2651.

15 (*a*) J. Yuan, X. Fang, L. Zhang, G. Hong, Y. Lin, Q. Zheng, Y. Xu, Y. Ruan, W. Weng, H. Xia and G. Chen, *J. Mater. Chem.*, 2012, **22**, 11515; (*b*) G. Hong, H. Zhang, Y. Lin, Y. Chen, Y. Xu, W. Weng and H. Xia, *Macromolecules*, 2013, **46**, 8649.

16 S. Bode, L. Zedler, F. H. Schacher, B. Dietzek, M. Schmitt, J. Popp, M. D. Hager and U. S. Schubert, *Adv. Mater.*, 2013, **25**, 1634.

17 Z. Wei, J. He, T. Liang, H. Oh, J. Athas, Z. Tong, C. Wang and Z. Nie, *Polym. Chem.*, 2013, **4**, 4601.

18 (*a*) E. V. Kirkby, J. D. Rule, V. J. Michaud, N. R. Sottos, S. R. White and J. A. Manson, *Adv. Funct. Mater.*, 2008, **18**, 2253; (*b*) S. Neuser, S. Michaud and S. R. White, *Polymer*, 2012, **53**, 370.

19 E. D. Rodriguez, X. Luo and P. T. Mather, *ACS Appl. Mater. Interfaces*, 2011, **3**, 152.

20 X. Luo and P. T. Mather, *ACS Macro Lett.*, 2013, **2**, 152.

21 J. Zhang, Y. Niu, C. Huang, L. Xiao, Z. Chen, K. Yang and Y. Wang, *Polym. Chem.*, 2012, **3**, 1390.

22 B. T. Michal, C. A. Jaye, E. J. Spence and S. J. Rowan, *ACS Macro Lett.*, 2013, **2**, 694.

23 H. Zhang and Y. Zhao, *ACS Appl. Mater. Interfaces*, 2013, **5**, 13069.

24 M. Behl and A. J. Lendlein, *J. Mater. Chem.*, 2010, **20**, 3335.

25 I. Bellin, S. Kelch, R. Langer and A. Lendlein, *Proc. Natl. Acad. Sci. U. S. A.*, 2006, **103**, 18043.

26 T. Ware, K. Hearon, A. Lonnecker, K. L. Wooley, D. J. Maitland and W. Voit, *Macromolecules*, 2012, **45**, 1062.

27 G. Li, G. Fei, H. Xia, J. Han and Y. Zhao, *J. Mater. Chem.*, 2012, **22**, 7692.

28 A. C. Jackson, F. L. Beyer, S. C. Price, B. C. Rinderspacher and R. H. Lambeth, *Macromolecules*, 2013, **46**, 5416.

29 J. R. Kumpfer, J. Jin and S. J. Rowan, *J. Mater. Chem.*, 2010, **20**, 145.

30 Y. H. Kim and R. P. Wool, A theory of healing at a polymer–polymer interface, *Macromolecules*, 1983, **41**, 1115.